

# **LEGIBILITY NOTICE**

**A major purpose of the Technical Information Center is to provide the broadest dissemination possible of information contained in DOE's Research and Development Reports to business, industry, the academic community, and federal, state and local governments.**

**Although a small portion of this report is not reproducible, it is being made available to expedite the availability of information on the research discussed herein.**

LA-UR -89-2342 . . .  
CONF-891214--3

Received by OSTI  
AUG 07 1989

Los Alamos National Laboratory is operated by the University of California for the United States Department of Energy under contract W-7405-ENG-36

LA-UR--89-2342

DE89 015265

TITLE: MESA 3-D CALCULATIONS OF ARMOR PENETRATION BY PROJECTILES WITH COMBINED  
OBLIQUITY AND YAW

AUTHOR(S): D. J. Cagliostro, X-3  
D. A. Mandell, X-3  
L. A. Schwalbe, X-3  
T. F. Adams, X-3  
E. J. Chapyak, X-3

SUBMITTED TO: 1989 Hypervelocity Impact Symp.  
San Antonio, TX  
Dec. 12-14, 1989

#### DISCLAIMER

This report was prepared as an account of work sponsored by an agency of the United States Government. Neither the United States Government nor any agency thereof, nor any of their employees, makes any warranty, express or implied, or assumes any legal liability or responsibility for the accuracy, completeness, or usefulness of any information, apparatus, product, or process disclosed, or represents that its use would not infringe privately owned rights. Reference herein to any specific commercial product, process, or service by trade name, trademark, manufacturer, or otherwise does not necessarily constitute or imply its endorsement, recommendation, or favoring by the United States Government or any agency thereof. The views and opinions of authors expressed herein do not necessarily state or reflect those of the United States Government or any agency thereof.

By acceptance of this article, the publisher recognizes that the U.S. Government retains a nonexclusive, royalty-free license to publish or reproduce the published form of this contribution or to allow others to do so, for U.S. Government purposes.

The Los Alamos National Laboratory requests that the publisher identify this article as work performed under the auspices of the U.S. Department of Energy.

 **Los Alamos** Los Alamos National Laboratory  
Los Alamos, New Mexico 87545

*[Handwritten signature]*

**MESA 3-D CALCULATIONS OF ARMOR PENETRATION  
BY PROJECTILES WITH COMBINED OBLIQUITY AND YAW**

by

D. J. Cagliostro, D. A. Mandell, L. A. Schwalbe,  
T. F. Adams, and E. J. Chapyak

Los Alamos National Laboratory  
Los Alamos, NM 87545

**SUMMARY**

We introduce and briefly describe MESA, a new 3-D hydrodynamic code, developed specifically for simulations of armor and anti-armor systems. The code's current capabilities and its planned model improvements and additions are discussed. An Eulerian code using state-of-the-art numerical methods, MESA runs faster and is less affected by spurious numerical diffusion than older codes. It models hydrodynamic flow and the dynamic deformation of solid materials. It uses simple elastic-perfectly plastic material strength models as well as models with strain and strainrate hardening and thermal softening. Future versions will incorporate advanced fracture models. It treats detonations in explosives using a programmed burn. The code's current capabilities are illustrated with simulations of experiments on yawed rods obliquely impacting armor plates at 1.29 km/s. With nominal elastic-perfectly plastic strength parameters MESA simulates well the experiment measurements of rod length and velocity deflection but not as well exit velocities and emergent rotation

rates. An artificial simulation of fracture indicates that fracture modeling would improve agreement with experiment. The utility of MESA to treat hypervelocity impacts is demonstrated with simulations of a rod obliquely impacting a thin plate at 5 km/s. The hypervelocity simulations show that hole sizes are much larger and that material strength plays a minor role in hole size and rod deformation at these higher velocities.

## INTRODUCTION

Yawed\* impacts can occur in many armor/anti-armor interactions. For example, in the oblique impact of an unyawed projectile into spaced armor the first layer deflects and rotates the projectile so that its interaction with the next layer becomes yawed. In reactive armor and flyover-shutdown situations, the relative velocity of the armor with respect to the penetrator can induce a yawed interaction. Simulations of these and other oblique and yawed impacts require 3-D hydrodynamics models.

In this paper we introduce and briefly describe the current and planned capabilities of a new 3-D hydrocode called MESA. We then compare simulations of yawed oblique impacts of long rods into thin plates with experiments, and finally demonstrate the utility of the code to simulate the hypervelocity impact of the penetrator into a thin plate. In the yawed oblique impacts, the rod strikes the plate at an entrance velocity of 1.29 km/s, and in the hypervelocity application at 5 km/s.

---

\* We use the term yaw as it was used by Fugelso and Taylor in [11] to describe what is commonly called pitch, the rotation of a body about an axis through its center of mass that lies in the horizontal plane and is perpendicular to its direction of travel.

This paper is divided into the following three main sections: The MESA Code, which gives an overview of the code, Yawed Oblique Impacts at Ordnance Velocities, which compares the code predictions with experiments, and Oblique Impacts at Hypervelocities, which demonstrates the code's utility to model impacts at much higher velocities and pressures.

### THE MESA CODE

MESA is a three-dimensional, Cartesian mesh, Eulerian code with hydrodynamics, high explosives, and material strength models. A companion 2-D code is available for scoping studies before doing detailed 3-D calculations, which take much more computer time. The two-dimensional algorithms have been described by Youngs [1]. The hydrodynamics is divided into two phases. The first phase is a pure Lagrangian calculation, and the second phase is a remapping back to the original Eulerian mesh. Since the advection (second phase) requires much more computer time than the first phase, the Lagrangian phase is sub-cycled. Typically we do four Lagrangian calculations for each remapping. Operator splitting is used in the material advection phase. That is, the calculations are done in the x, y, and z-directions during one time cycle, and then in the z, y, and x-directions during the next cycle. Van Leer [2] limiting is also used in the advection to maintain steep gradients of advected variables without introducing nonphysical oscillations.

A unique feature of MESA is the interface reconstruction algorithm, which was developed by David Youngs [3] of the UK Atomic Weapons Establishment. This model allows fewer cells to be used for the same accuracy than in earlier codes because mixed-cell material interfaces are calculated accurately. The interface reconstruction method assures that materials are advected in the correct order.

Material strength modeling is possible with a variety of yield models using a von Mises flow criterion. Yield models include the elastic-perfectly plastic model, the Steinberg-Cochran-Guinan model [4] with work hardening and thermal softening, and the Johnson-Cook [5] model with strain-rate hardening in addition. A ductile fracture model is being implemented into the code [6]. A ductile and brittle fracture model (an extension of the TEPLA model [7]) is being developed and will be implemented later.

We use the standard JWL [8] equation of state (EOS) for the high explosive (HE) and currently treat detonations with a programmed burn model in which the burn time interval for each cell is calculated in the setup phase using the high explosive detonation velocity and a Huygens construction. A coupled hydro-HE model (Johnson-Tang-Forest [9]) will be implemented in the future.

In addition to the JWL EOS for the HE detonation products, a number of analytical EOS equations are available for other materials. The Los Alamos tabular equations-of-state, SESAME [10], are also available.

MESA currently runs on Cray X-MP and Y-MP computers. To run efficiently in a time sharing environment, dynamic memory management is used. Thus, for any given calculation, only the amount of computer memory needed for that application is required.

## YAWED OBLIQUE IMPACTS AT ORDNANCE VELOCITIES

We used MESA to model the oblique impact of yawed kinetic energy projectiles into thin plates. Figure 1 shows the orientation of the rod axis and velocity vector relative to a stationary plate for  $+10^\circ$ ,  $0^\circ$ , and  $-10^\circ$  yaw at an obliquity of  $65^\circ$ . If we define obliquity,  $\gamma$ , as the angle between the rod velocity vector and the

plate normal in a coordinate system fixed to the plate, and  $\beta$  as the angle between the rod axis and the plate normal, then the yaw angle,  $\alpha$ , equals  $\gamma - \beta$ . In other words, in the reference frame of the plate the yaw angle is simply the angle between the rod axis and velocity vector.

The objectives of these calculations are to determine the effects of both positive and negative yaws on the oblique impact of penetrators into thin plates and to compare the predictions with experiments. Our approach is to model the experiments that were performed and described by Fugelso and Taylor [11] on the oblique impact of yawed uranium alloy rods into thin steel plate.

#### Description of the Experiments

In the experiments, stable yawed impacts were achieved by moving the target plate obliquely in the path of a horizontally fired rod having little, if any, inherent initial yaw. Figure 2 shows the rod-plate orientations for the three yaw cases modeled here along with their initial velocities. Negative yaw was produced by moving the plate toward the projectile; positive yaw was produced by moving the plate away from the projectile. The plate was accelerated by detonating a thin layer of sheet explosive attached to one surface.

The penetrators were cylindrical rods made of U-0.75 wt% Ti and were 7.67 cm long with a hemispherical tip, an aspect ratio ( $L/D$ ) of 10, and a mass of 65 g. The plates were made of 6.4-mm-thick rolled homogeneous armor (RHA) (BHN  $\approx$  370). The initial velocities and orientations of the rods and plates were designed so that the rod impact velocity relative to the plate was 1.29 km/s at an obliquity of  $65^\circ$  for each of the three nominal yaws of  $-10^\circ$ ,  $0^\circ$  and  $+10^\circ$ .

### Modeling the Experiments

For the rod and plate materials, we used the Mie-Grüneisen EOS referenced to their measured Hugoniot states and initial densities of  $18.62 \text{ g/cm}^3$  and  $7.896 \text{ g/cm}^3$ , respectively. The material strength was modeled with an elastic-perfectly plastic model and the von Mises yield criterion. The constant yield stress for the U-0.75 wt% Ti was 17.9 kbars and for the RHA 10.0 kbars, based on the material strength measurements given in [12] and [5], respectively. We anticipated the importance of plate fracture in this problem, but because the code has no fracture model, we could only investigate the effect approximately. Therefore, we simulated fracture in one of the problems by stopping the calculation at a time we believe the plate would have failed. Then we removed plate material in contact with the rod, manually restarted the calculation, and ran it to completion.

We used 1-mm mesh cells in the region of impact and a geometrically expanding mesh out to the grid boundaries. The geometrical expansion factor was 1.1. Taking advantage of the plane of symmetry in these experiments, we modeled only half the geometry and required 202,752 cells --- 132 cells in the x direction (21.5 cm), 48 cells in the y direction (8 cm), and 32 cells in the positive z direction (5 cm). The simulations to 100  $\mu\text{s}$  required only about three hours of CPU time on a Cray X-MP computer. A post processor was written to calculate the length, center-of-mass velocity, velocity deflection, and angular velocity of the rod for each dump time.



## RESULTS

### Effects of Yaw

The qualitative experimental results of the trajectory deflection and yaw rate of the emergent rod are shown in Fig. 3. This figure also shows the sign convention used to describe the rod trajectory deflection and yaw rate.

Cross sectional views of the interfaces between the rod and the plate at 50 and 100  $\mu\text{s}$  after start of the calculations are shown in Fig. 4 for the  $-9.3^\circ$ ,  $0^\circ$ , and  $+10^\circ$  yaw cases. The cross sections are through the cells next to the plane of bilateral symmetry (at the  $z=1$  cell level). These views show that the rods deform mainly in the region of the rod tip and that no significant bending occurs elsewhere. The "taffy-like" appearance of the plate underneath the rod is an artifact resulting from our present inability to model fracture adequately. For  $-9.3^\circ$  yaw, the rod deflects upward, away from the normal to the back surface of the plate, for  $0^\circ$  yaw, it deflects slightly, and for  $+10^\circ$  yaw, it deflects downward, toward the plate normal.

The MESA code predictions of velocity, deflection, and rotation rate of the rod as it penetrates and exits the plate are shown in Figs. 5, 6, and 7, respectively. Figure 5 shows that maximum reduction in velocity occurs for  $-9.3^\circ$  yaw ( $V/V_i = 0.68$  at 100  $\mu\text{s}$ ). Corresponding velocity reductions for the  $0^\circ$  and  $10.3^\circ$  yawed rods are comparable to each other ( $V/V_i = 0.80$  at 100  $\mu\text{s}$ ) but less than that for the negative yaw case. Predictions of rod deflections (Fig. 6) show that initially in all three cases the rod deflects upward, away from the plate normal. Later, for  $-9.3^\circ$  yaw the rod continues to deflect away from the plate normal; whereas in the other two cases the rod deflects toward the plate normal with the larger deflection occurring for  $+10.3^\circ$  yaw. Predictions of rod rotation rates (Fig. 7) show

again that in all three cases the rod is initially rotating away from the plate normal, but by the time the rod exits the plate it is rotating toward the plate normal, in each case at about the same rate of  $0.18^\circ/\mu\text{s}$  at  $t = 100 \mu\text{s}$ .

### Comparisons with Experiments

MESA predictions of rod length, velocity, deflection, and rotation rate at  $t=100 \mu\text{s}$ , after the rod has emerged from the plate, are compared with the experiment measurements in Figs. 8, 9, 10, and 11, respectively. Figure 8 shows that the final rod lengths are about the same for each of the three yaw cases and agree well with the experiments. MESA predictions of exit velocities (Fig. 9), however, are about 15% lower than those measured in the experiments. The calculation with "fracture" at  $50 \mu\text{s}$  gives better agreement with experiment and indicates the importance of modeling fracture. The predictions of trajectory deflection (Fig. 10) agree well with the experiments and again the calculation with fracture agrees even better. As shown in Fig. 11, however, MESA predicts rod rotation rates much greater than those measured in the experiments. As indicated, however, by the significant scatter in the measurements these rotation rate measurements are very difficult to make accurately and are not very repeatable.

## OBLIQUE HYPERVELOCITY IMPACTS

### Modeling the Impact

As an example of an application of MESA to a hypervelocity impact, we chose to model the  $0^\circ$  yaw impact experiment described above using the same geometry, material strength models, and yield stresses, but with the Sesame EOS and with the rod velocity increased from 1.29 to 5 km/s. The tabulated Sesame EOS was used to allow calculation of temperatures in the rod and plate which we could not do directly with the Mie-Grüneisen EOS. (Comparisons of inter-

face plots at exit time using the Sesame EOS agreed very well with those using the Mie-Grüneisen EOS. The choice of EOS, therefore, does not affect the geometry or dynamics of the problem significantly.)

### Results

Figure 12 compares the interface plots at 10 and 25  $\mu\text{s}$  for the hypervelocity impact with those for the ordnance velocity impact at 40 and 100  $\mu\text{s}$  (times scaled inversely to initial rod velocity). The main effect of going to hypervelocity is to increase the size of the hole in the plate. Also, the deformation and bending of the rod are significantly less noticeable in the hypervelocity impact in which material strength is less important.

To see the reduced importance of strength in a hypervelocity impact, Fig. 13 compares the MESA predictions with and without material strength. At these high velocities there is very little effect of strength on hole size, being only slightly smaller with strength. The rod tip is slightly less deformed and eroded with strength than without strength.

Figure 14 compares the hypervelocity impact with the ordnance velocity impact without strength. The comparison shows that the hole size at scaled times are the same. This agrees with scaling laws for impacts of incompressible fluids.

### CONCLUSIONS

We have shown that in modeling yawed oblique impacts of long rods into thin plates at 1.29 km/s the 3-D MESA hydrocode:

- Predicts well rod lengths and trajectory deflections.

- Predicts greater attenuation of velocity than that measured in the experiments.

**Predicts much higher emergent yaw rates than those measured in the experiments.**

**Agrees better, in general, when fracture is simulated.**

**We have also demonstrated MESA modeling of a hypervelocity oblique impact at 5 km/s. In these calculations we have shown the significant differences between ordnance impact and hypervelocity impact, the relative unimportance of material strength in such hypervelocity impacts compared with the importance of material strength in ordnance velocity impacts, and that the code predictions scale as expected when strength is not important.**

**To better understand the effects of cell size, material strength models, and fracture on modeling yawed impacts, we plan to do the following:**

- 1. Increase the cell size to about 1.2 mm in the -9 3° yaw case to see if we get the same results with fewer cells or if we need an even greater number of cells.**
- 2. Apply the Johnson-Cook strength model to determine the effects of strain hardening and thermal softening.**
- 3. Apply the ductile and brittle fracture model (TEPLA) when it is implemented in MESA. Based on the results shown here, we think that being able to model fracture will significantly improve the MESA predictions of velocity attenuation and emergent rod rotation rate.**

## ACKNOWLEDGMENTS

The 3-D MESA hydrocode was developed at the Los Alamos National Laboratory with DARPA/Army/Marine Corps support. Jim Lewis and Connie Wilson made the interface illustrations.

## REFERENCES

1. D. L. Youngs, "Time Dependent Multi-Material Flow With Large Fluid Distortion", in Morton, K. W. and Baines, J. H., ed., Numerical Methods for Fluid Dynamics, Academic Press (1982).
2. B. Van Leer, "Towards the Ultimate Conservative Difference Scheme." V.A Second-Order Sequel to Godunov's Method, J. of Comp. Phy., 32, pp.101-136 (1979).
3. D. L. Youngs, "An Interface Tracking Method for a 3-D Eulerian Hydrodynamics Code", UK Atomic Weapons Establishment, AWRE/44/92/35 (1987).
4. D. J. Steinberg, S. G. Cochran., and M. W. Guinan, "A Constitutive Model for Metals Applicable at High-Strain Rate", J. Appl. Phy. 51 (3), pp 1498-1504 (1980).
5. G. R. Johnson, and W. H. Cook., "A Constitutive Model and Data for Metals Subjected to Large Strains, High Strain Rates and High Temperatures", Seventh International Symposium on Ballistics, The Hague, The Netherlands (1983).
6. J. N. Johnson, "Dynamic Fracture and Spallation in Ductile Solids," J. App. Phy. 52 (4) pp 2812-2825 (1981).

7. J. N. Johnson, and F. L. Addessio, "Tensile Plasticity and Ductile Fracture", J. Appl. Phy. 64 (12), pp 6699-6712 (1988).
8. E. L. Lee, H. C. Hornig, and J. W. Kury, "Adiabatic Expansion of High Explosive Detonation Products", Lawrence Livermore National Laboratory Report, UCRL-50422 (May, 1968).
9. P. K. Tang, "Initiation and Detonation of Heterogeneous High Explosives: A Unified Model", Los Alamos National Laboratory Report LA-11352-MS (September, 1988).
10. C. W. Cranfill, "EOSPAC: A Subroutine Package for Accessing the Los Alamos SESAME EOS Data Library", Los Alamos National Laboratory Report, LA-9728-M (August, 1983).
11. E. Fugelso and J. W. Taylor, "Evaluation of Obliquity and Yaw for U 0.75 wt% Ti Penetrators," Los Alamos Scientific Laboratory report LA-7402-MS (July 1978).
12. J. W. Hopson, L. W. Hantel, and D. J. Sandstrom, "Evaluation of Depleted-Uranium Alloys for Use in Armor-Piercing Projectiles," Los Alamos Scientific Laboratory report LA-5238 (1973).

## FIGURES

- Figure 1. Rod-plate geometries for positive, zero, and negative yawed oblique impacts.
- Figure 2. Schematic of rod-plate orientations and initial velocities in the controlled yaw experiments.
- Figure 3. Qualitative results from the controlled yaw experiments and sign convention.
- Figure 4. Interface plots for (a)  $-9.3^\circ$ , (b)  $0^\circ$ , and (c)  $10.3^\circ$  yaw at  $50\text{ }\mu\text{s}$  (solid line) and  $100\text{ }\mu\text{s}$  (dashed line) after start of computations.
- Figure 5. Rod velocity histories.
- Figure 6. Rod trajectory deflection histories.
- Figure 7. Rod rotation histories.
- Figure 8. MESA predictions of final rod length compared with experiments.
- Figure 9. MESA predictions of rod exit velocities compared with experiments.
- Figure 10. MESA predictions of rod deflections compared with experiments.
- Figure 11. MESA predictions of rod rotation rates compared with experiments.
- Figure 12. Superimposed interface plots of (a) hypervelocity impact at  $5\text{ km/s}$  at  $10\text{ }\mu\text{s}$  (solid line) and  $25\text{ }\mu\text{s}$  (dashed line) compared with (b) ordnance velocity impact at  $1.29\text{ km/s}$  at  $40\text{ }\mu\text{s}$  (solid line) and  $100\text{ }\mu\text{s}$  (dashed line).
- Figure 13. Superimposed interface plots of hypervelocity impacts with strength (solid lines) and without strength (dashed lines) at (a)  $10\text{ }\mu\text{s}$  and (b)  $25\text{ }\mu\text{s}$ .
- Figure 14. Superimposed interface plots of (a) hypervelocity impact at  $5\text{ km/s}$  with strength at  $10\text{ }\mu\text{s}$  (solid line) and  $25\text{ }\mu\text{s}$  (dashed line) compared with (b) ordnance velocity impact at  $1.29\text{ km/s}$  without strength at  $40\text{ }\mu\text{s}$  (solid line) and  $100\text{ }\mu\text{s}$  (dashed line).

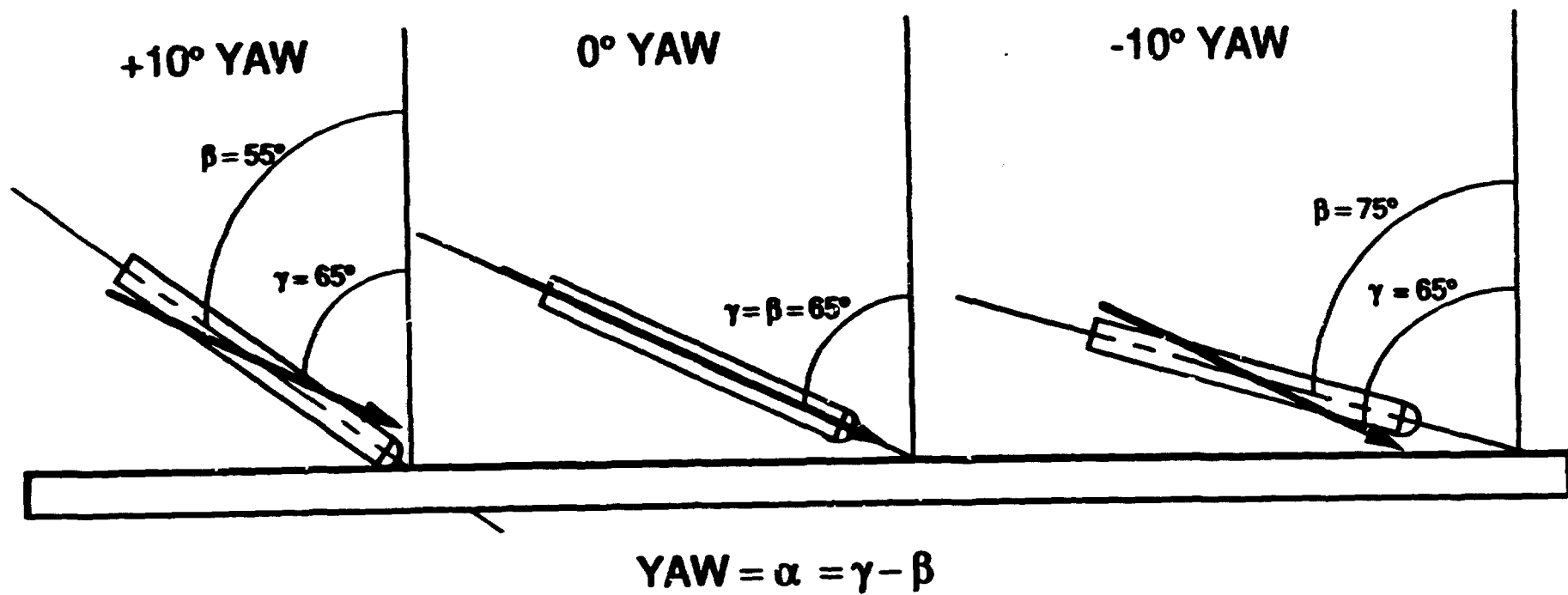


Fig. 1. Rod-plate geometries for oblique impacts at positive, zero, and negative yaws.



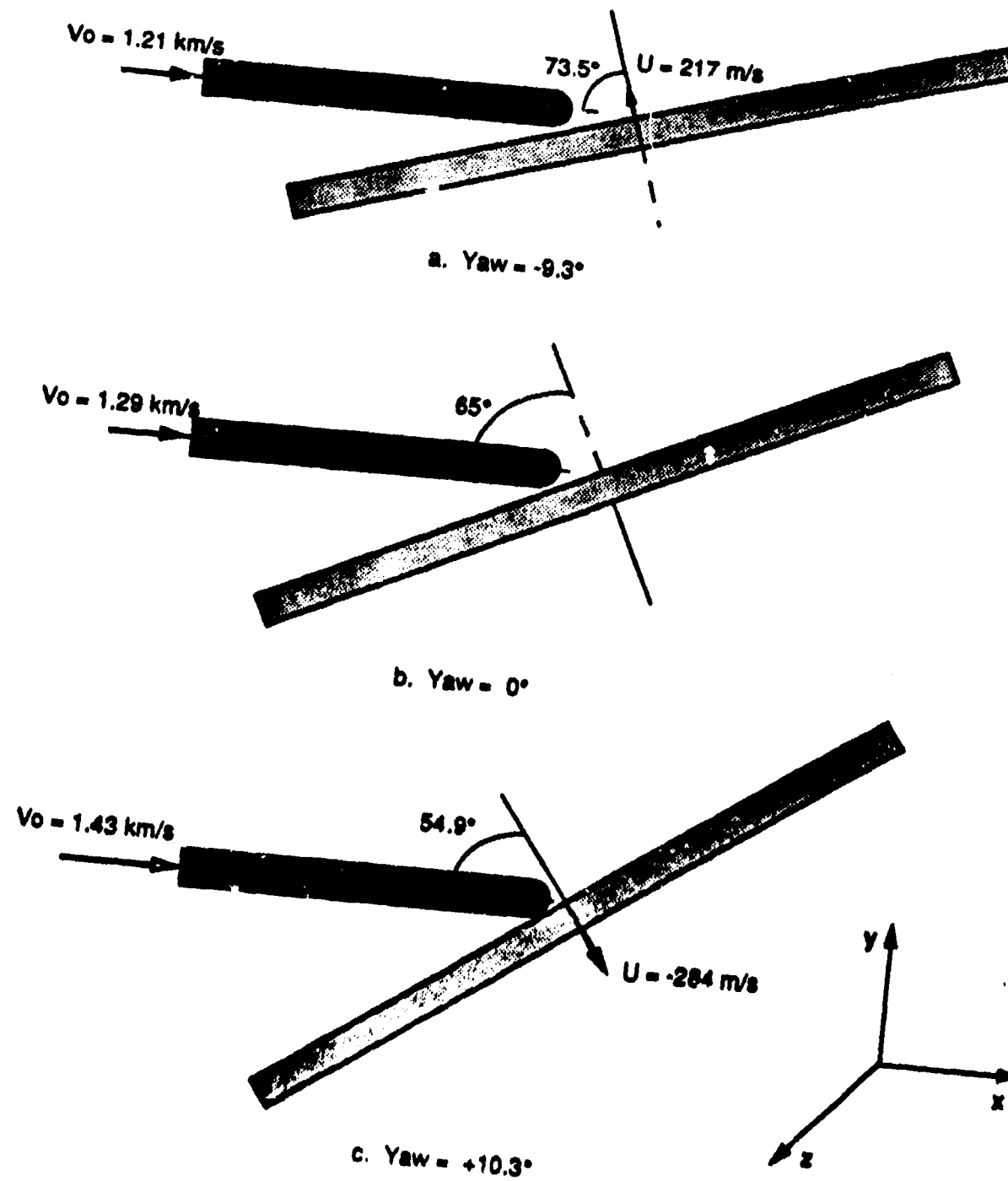
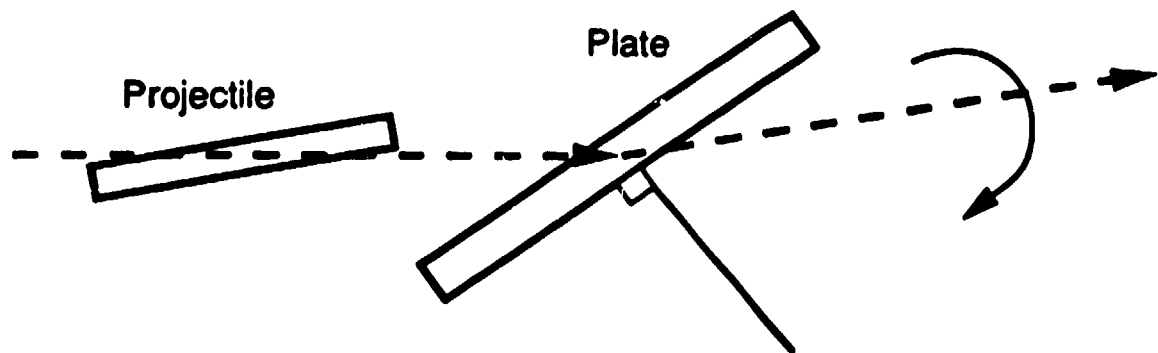
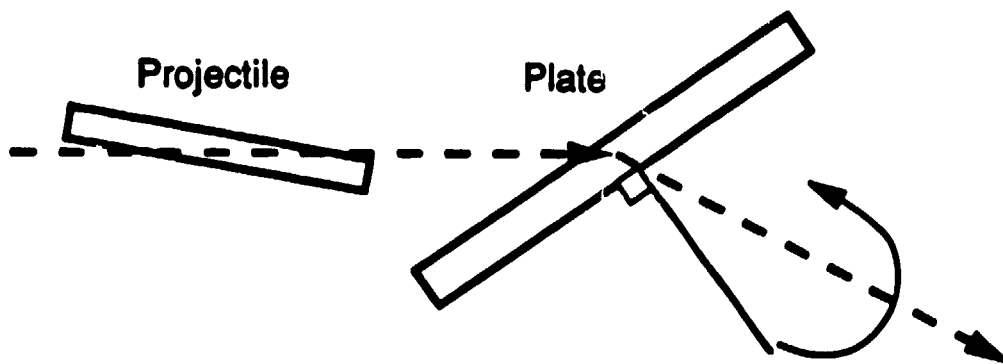


Fig. 2. Schematic of rod-plate orientations and initial velocities in the controlled yaw experiments.

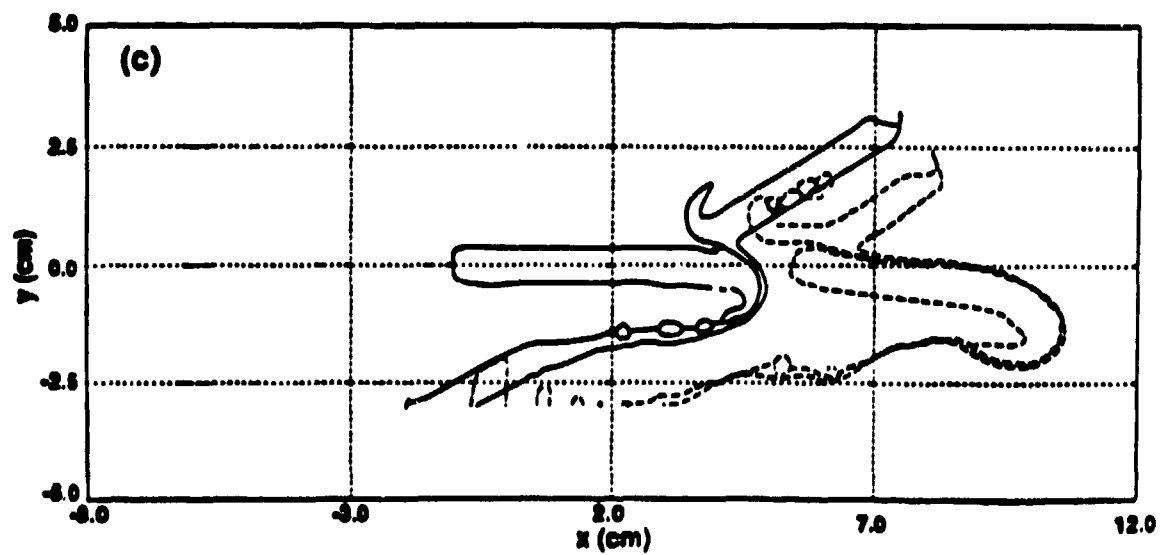
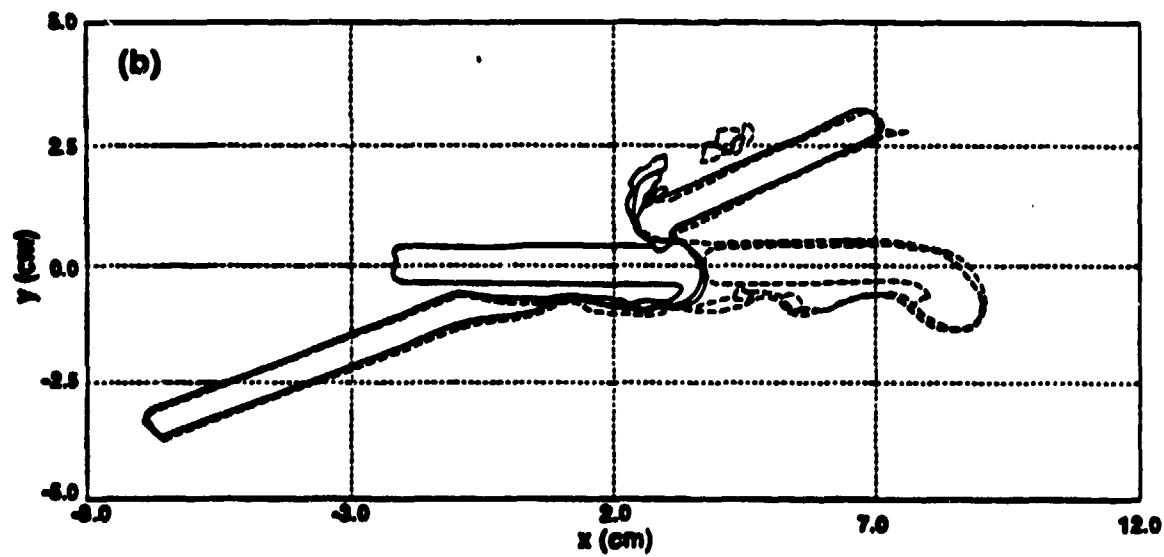
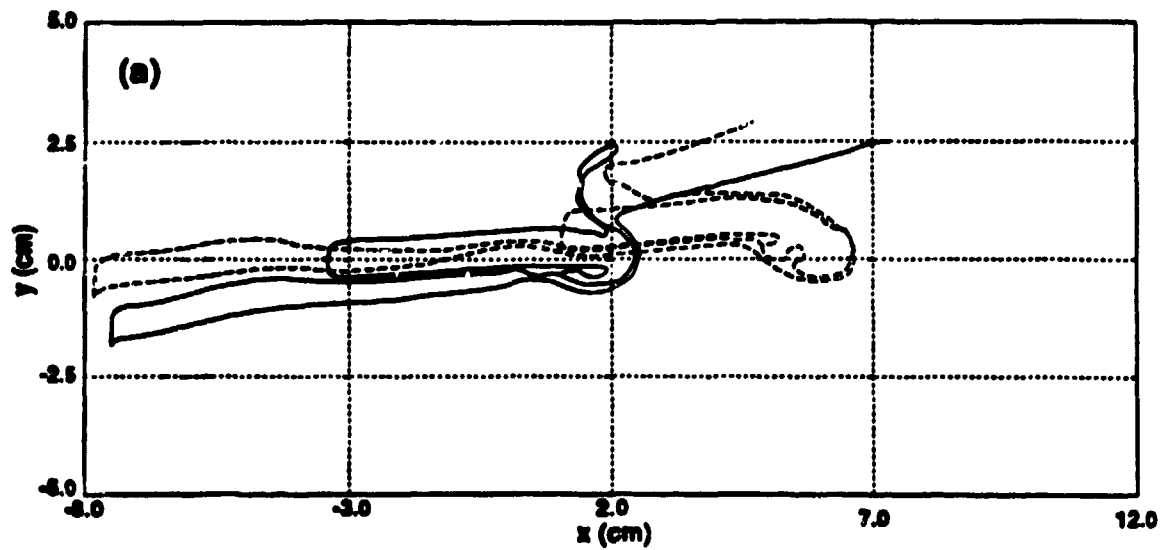


**Negative Yaw  $\Rightarrow$  Negative Trajectory Deflection + Positive Yaw Rate**



**Positive Yaw  $\Rightarrow$  Positive Trajectory Deflection + Negative Yaw Rate**

***Fig. 3. Qualitative results from the controlled yaw experiments and sign convention.***



✓  
Cagliostro Figure 2. Interface plots for (a) -9.3 yaw, (b) 0 yaw, and (c) +10.3 yaw. Solid line denotes position at 50  $\mu$ s, dashed line at 100  $\mu$ s.

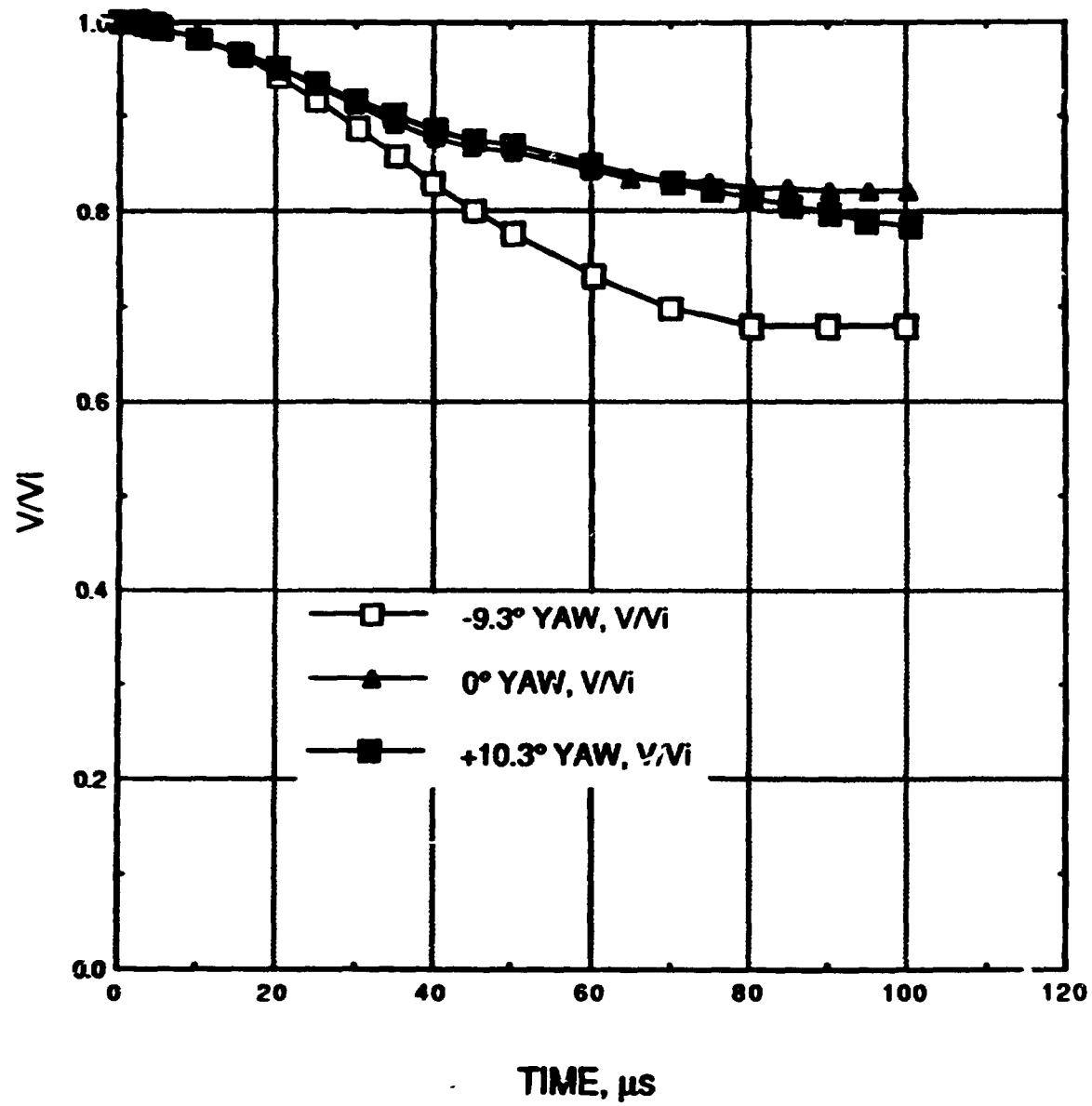


Fig. 5. Rod velocity histories.

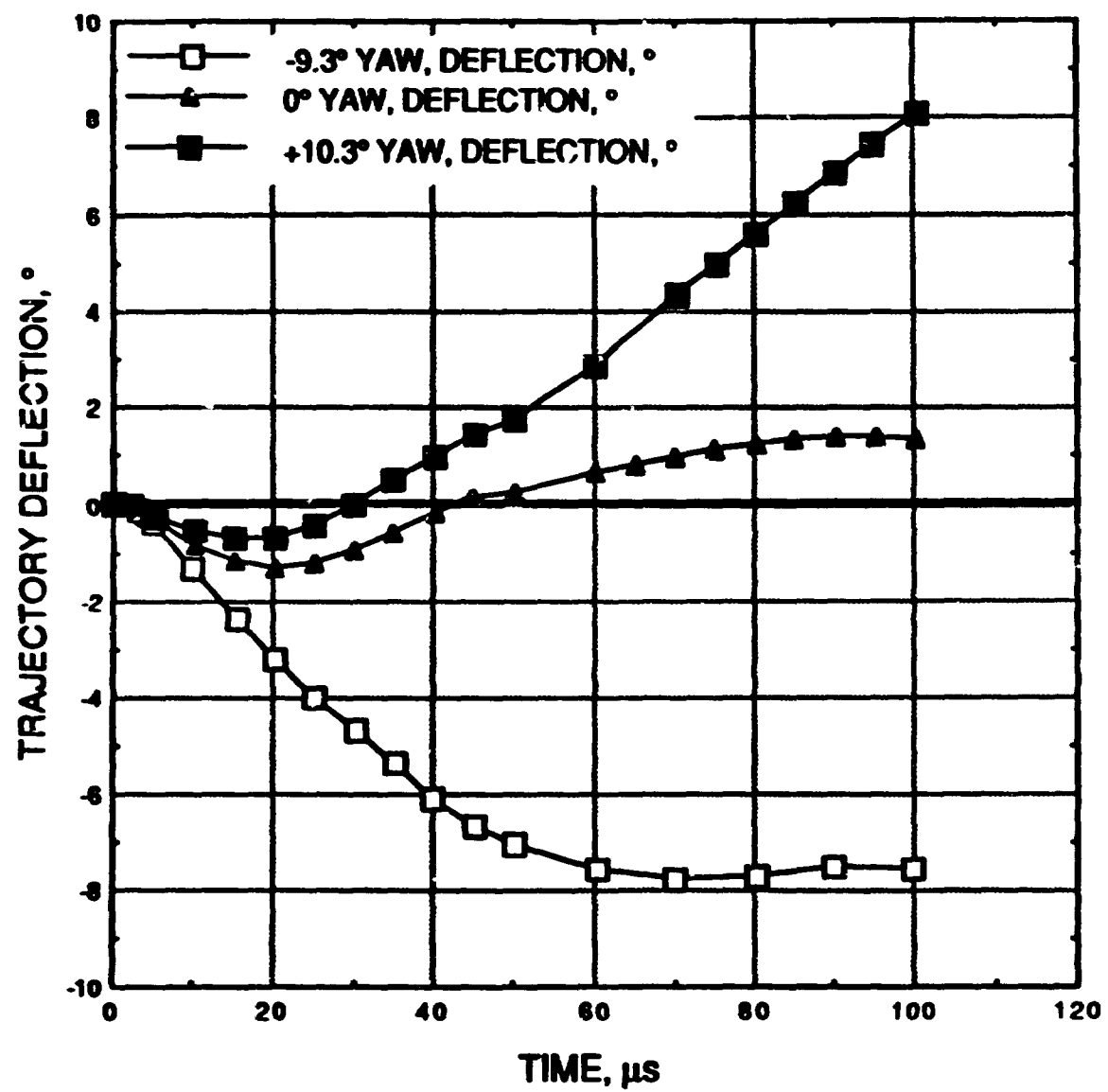


Fig. 6. Rod trajectory deflection histories.

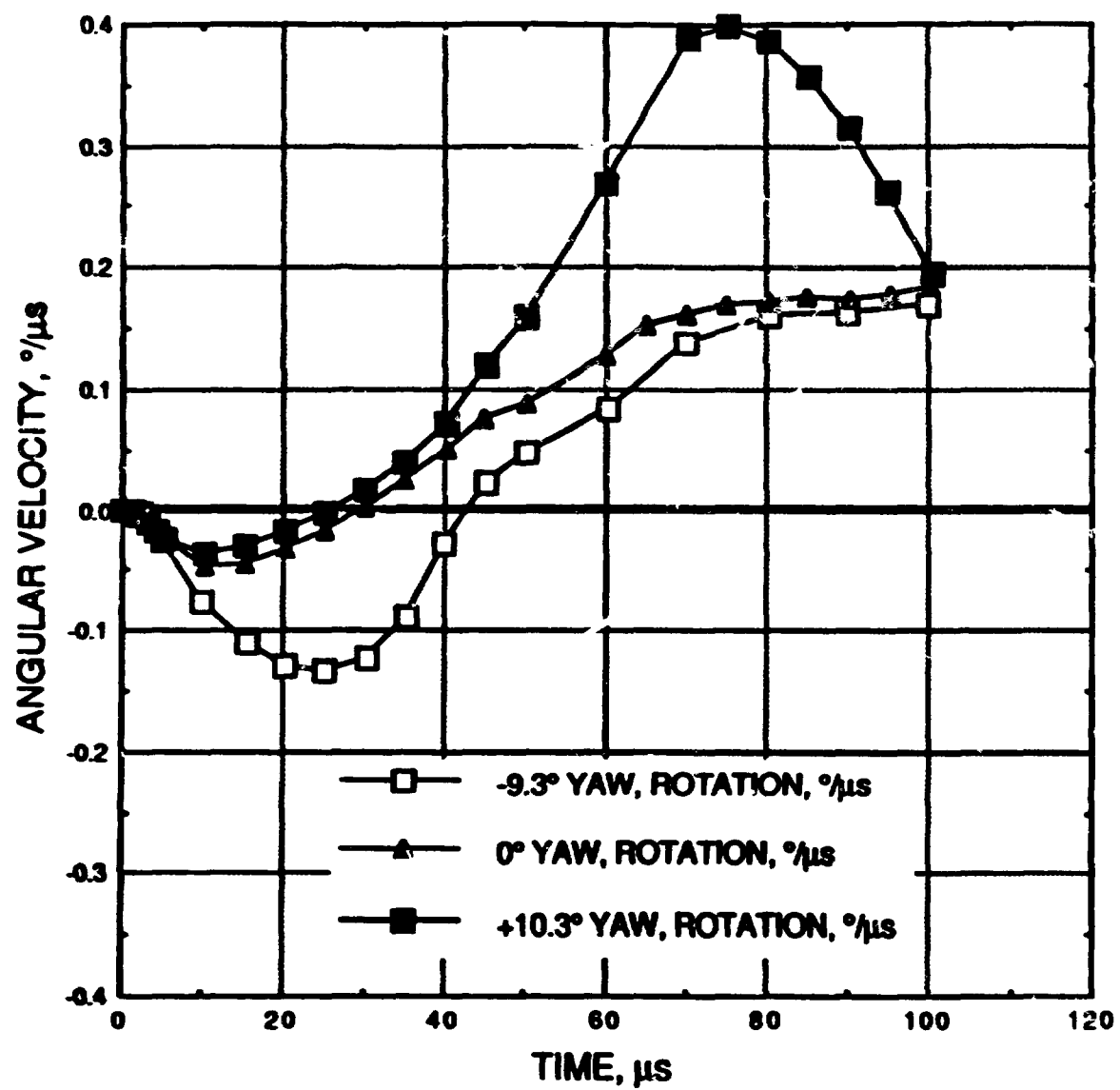


Fig. 7. Rod rotation histories.

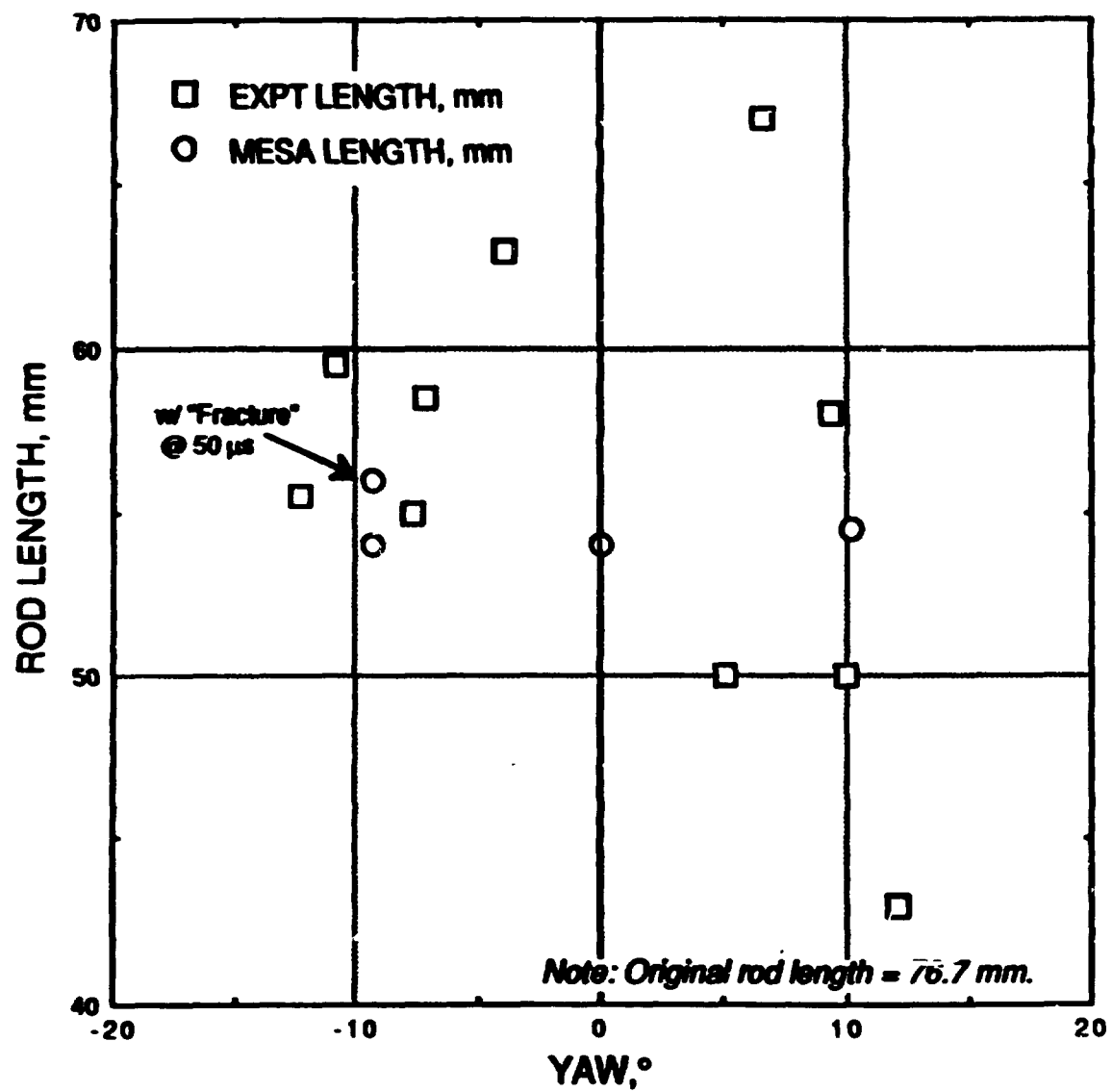
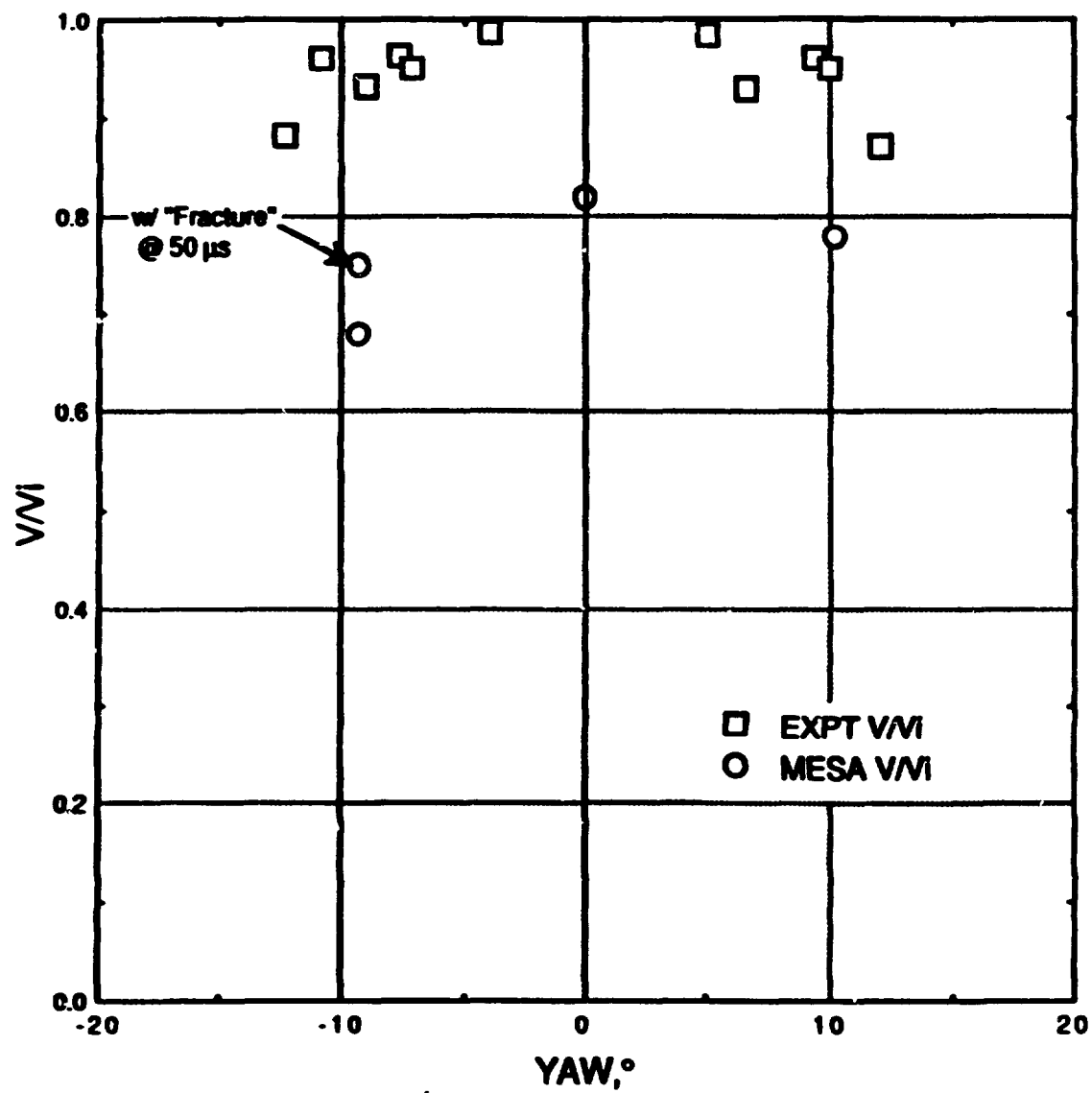


Fig. 8. MESA predictions of final rod length compared with experiments.



**Fig. 9. MESA predictions of rod exit velocities compared with experiments.**



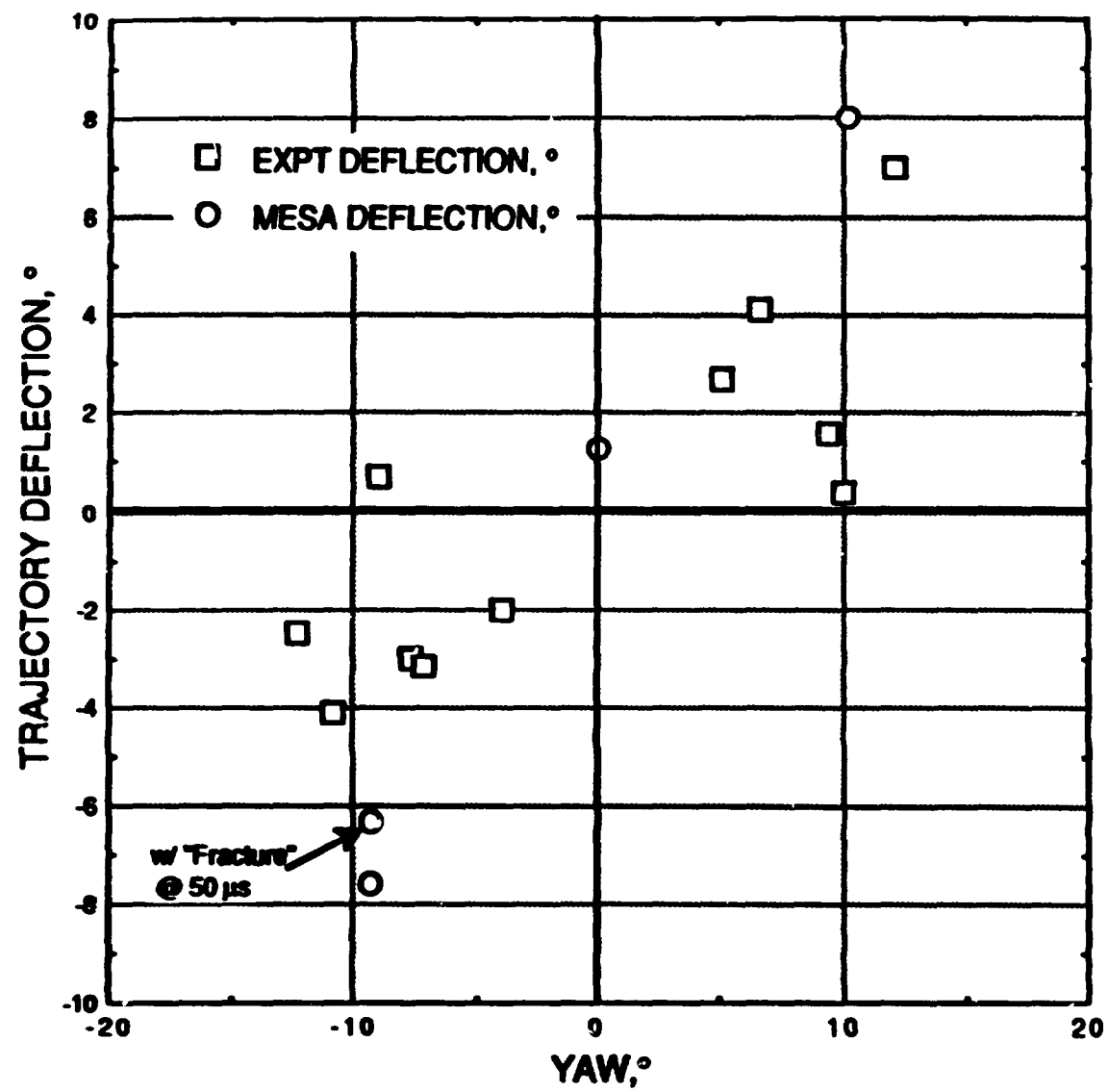


Fig. 10. MESA predictions of rod trajectory deflections compared with experiments.

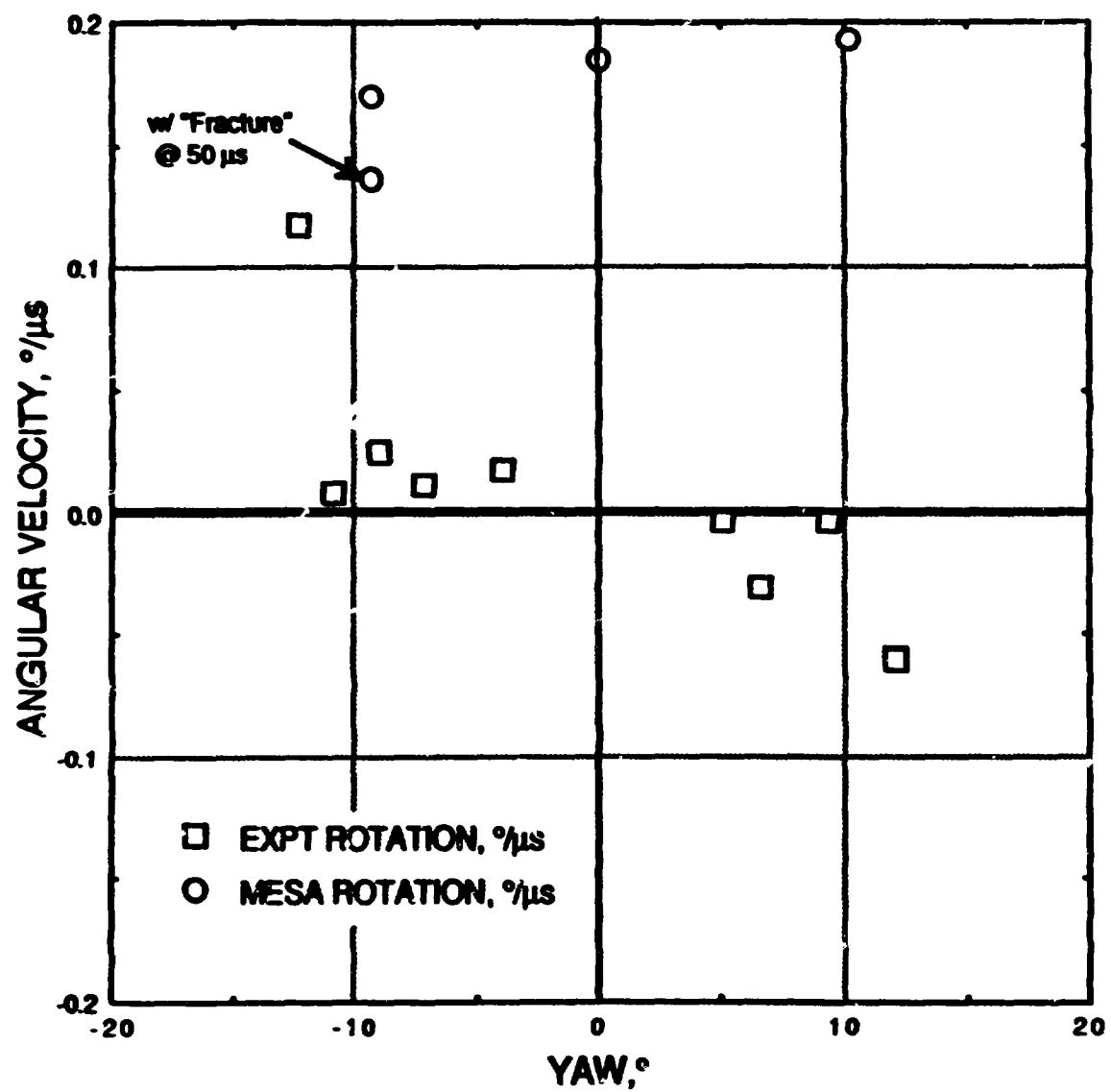


Fig 11. MESA predictions of rod rotation rates compared with experiments.

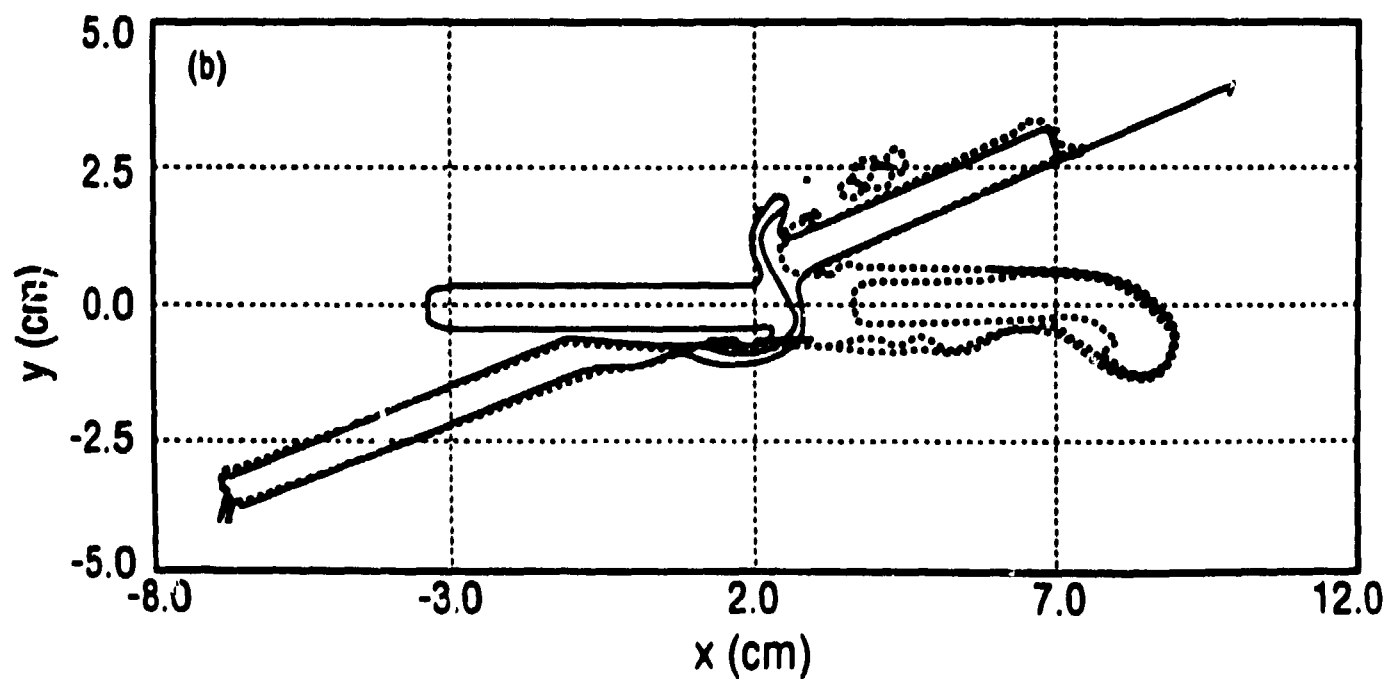
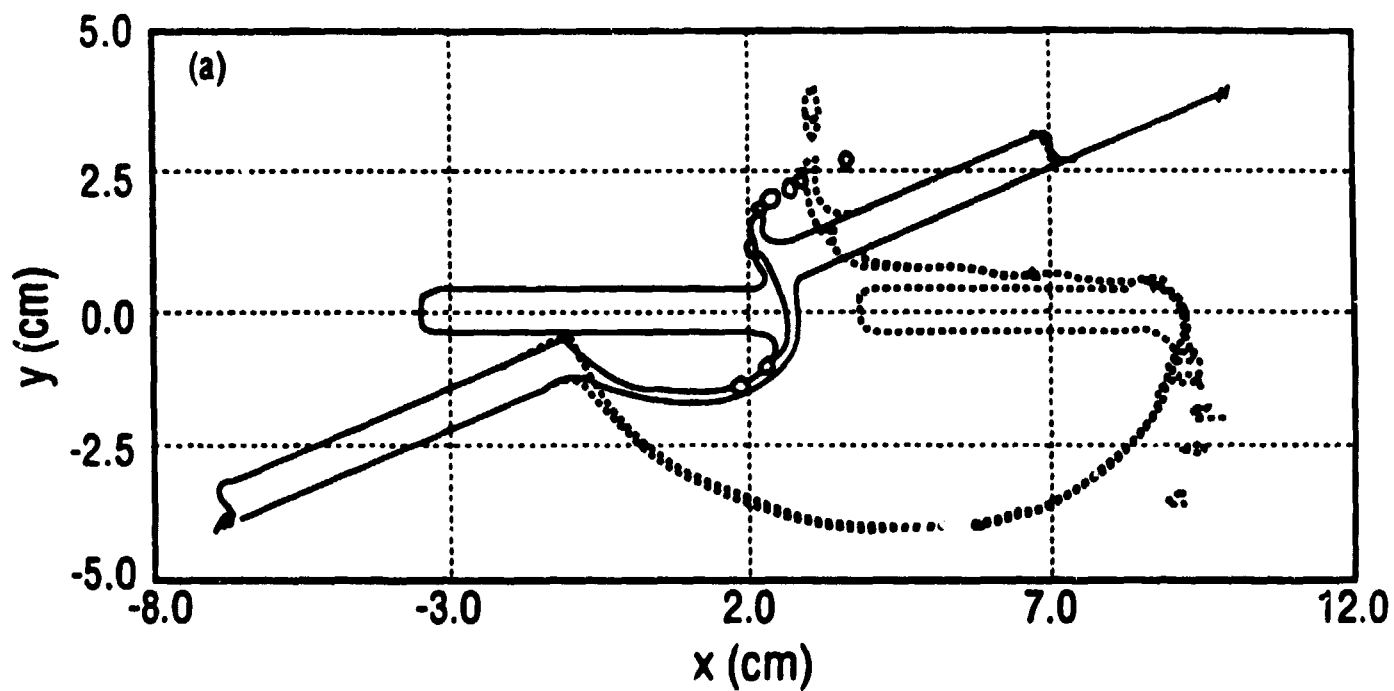


Fig. 12. Superimposed interface plots of (a) hypervelocity impact at 5 km/s at 10  $\mu$ s (solid line) and 25  $\mu$ s (dashed line) compared with (b) reference velocity.

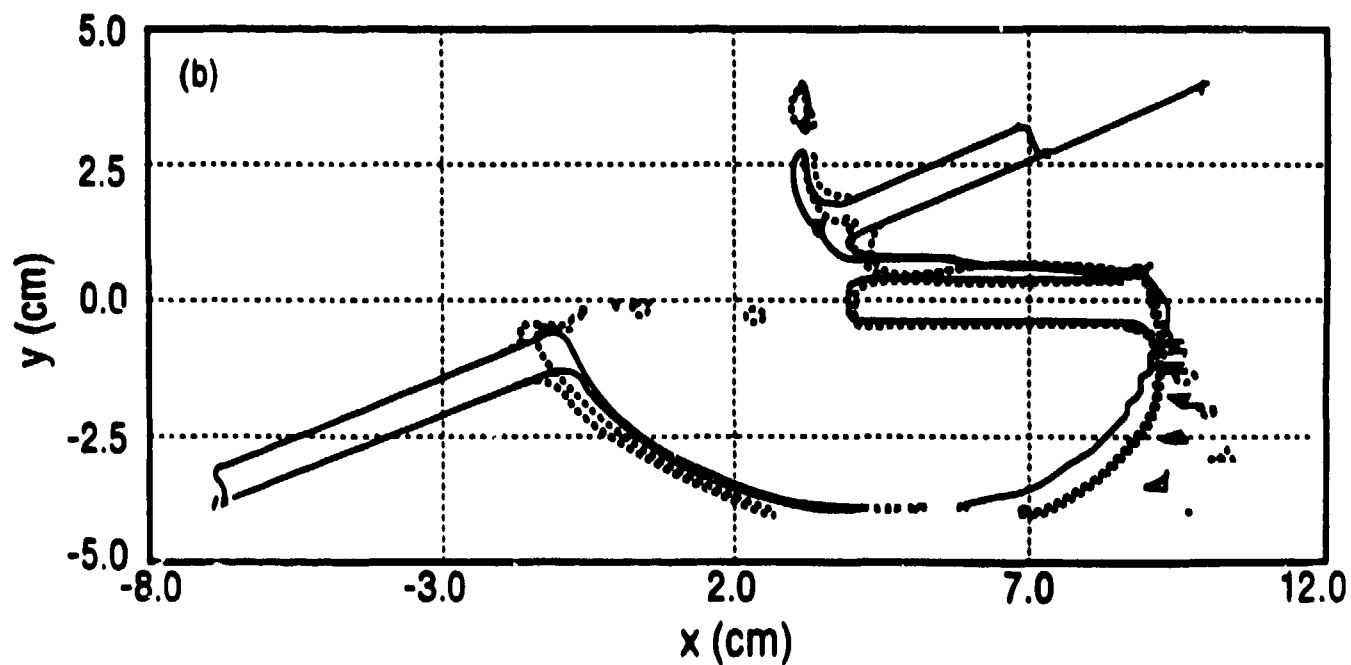
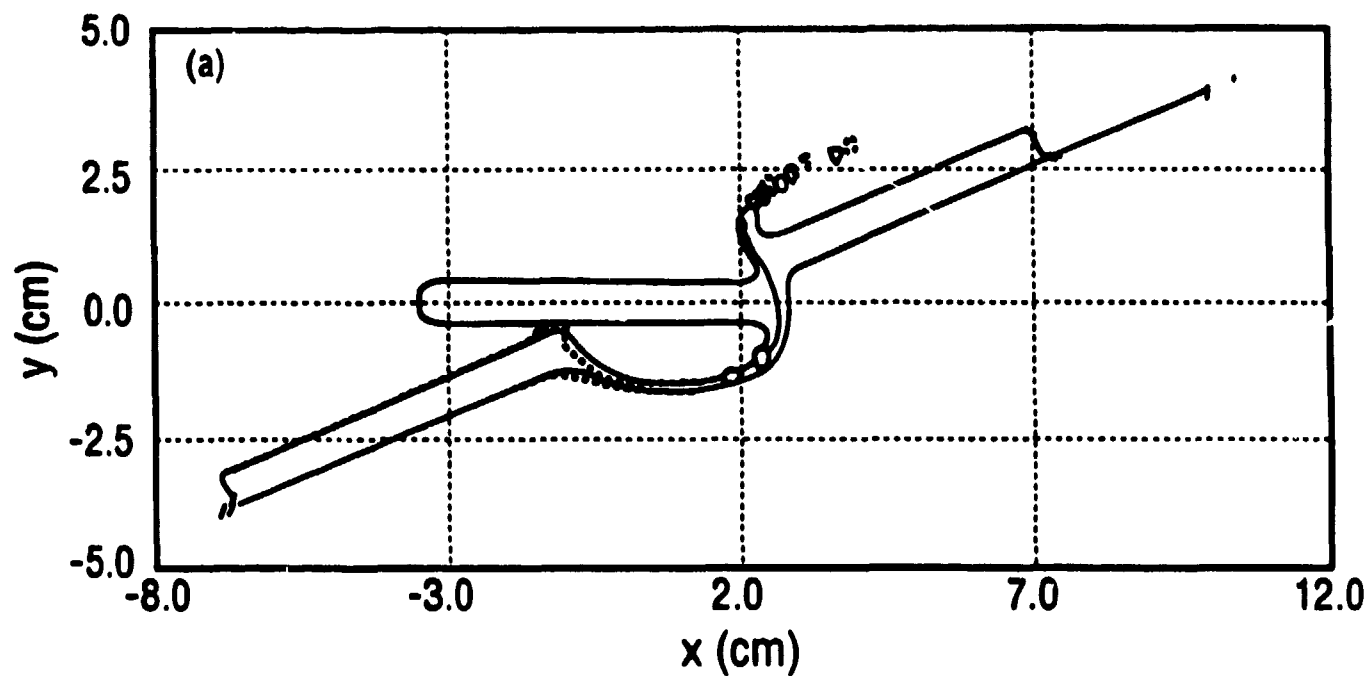


Fig. 13. Superimposed interface plots of hypervelocity impacts with strength (solid lines) and without strength (dashed lines) at (a)  $10 \mu s$  and (b)  $25 \mu s$ .

15a 8/1/85

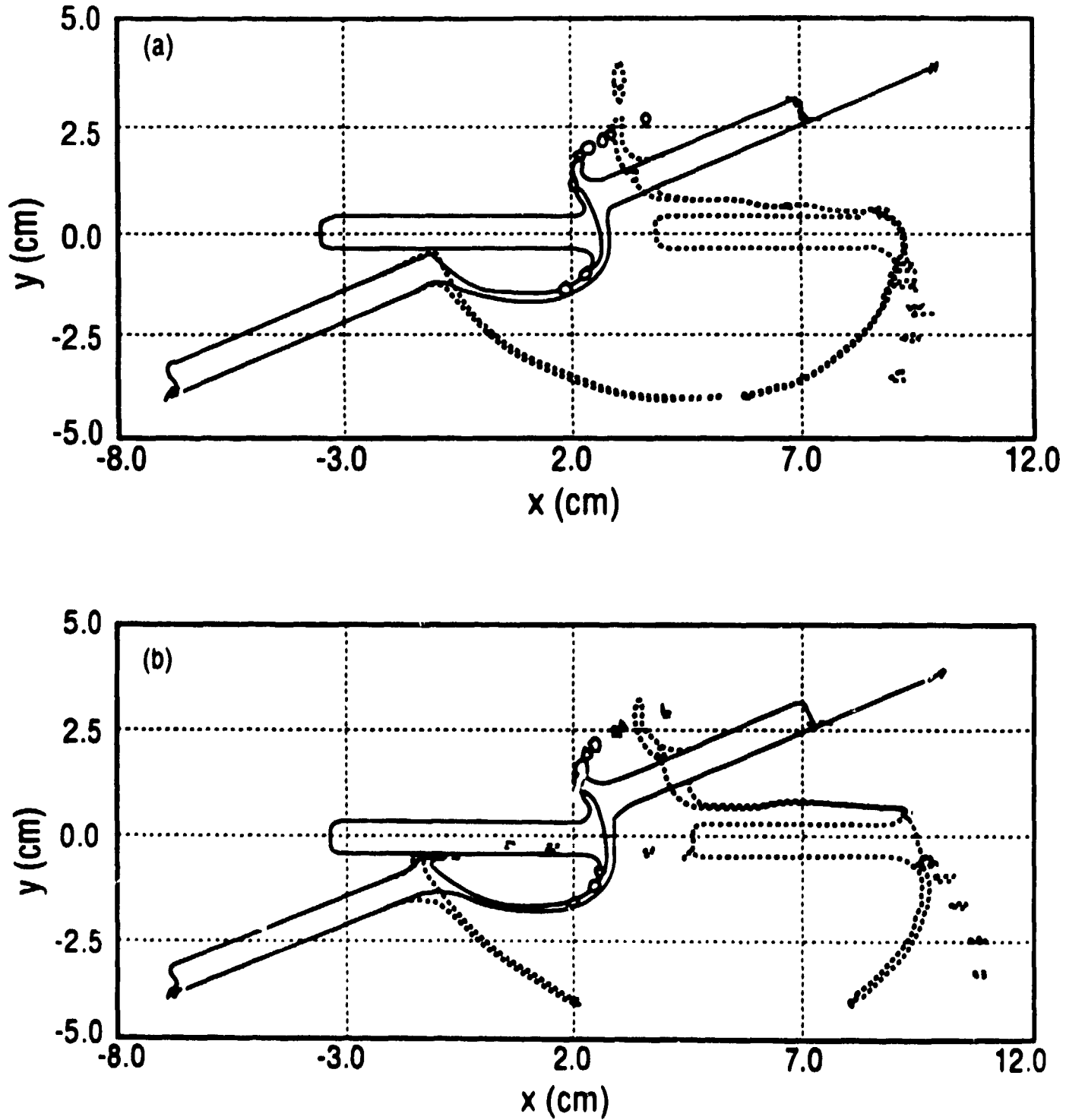


Fig. 14. Superimposed interface plots of (a) hypervelocity impact at 5 km/s with strength at 10  $\mu$ s (solid line) and 25  $\mu$ s (dashed line) compared with (b) ordnance velocity impact at 1.29 km/s without strength at 40  $\mu$ s (solid line) and 100  $\mu$ s (dashed line).